Time-resolved x-ray imaging of magnetization dynamics in spin-transfer torque devices

V. Chembrolu,[1,2] J. P. Strachan,[1,2] X. W. Yu,[1,2] A. A. Tulapurkar,[2] T. Tyliszczak,[3] J. A. Katine,[4] M. J. Carey,[4] J. Stöhr,[2,5] and Y. Acremann[2,6]

[1]*Department of Applied Physics, Stanford University, Stanford, California 94305, USA*
[2]*SIMES Institute, Stanford Linear Accelerator Center, Menlo Park, California 94025, USA*
[3]*Advanced Light Source, Berkeley, California 94720, USA*
[4]*Hitachi Global Storage Technologies San Jose Research Center, San Jose, California 95120, USA*
[5]*Stanford Synchrotron Radiation Lightsource, Menlo Park, California 94025, USA*
[6]*PULSE Institute, Stanford Linear Accelerator Center, Menlo Park, California 94025, USA*

(Received 15 February 2009; revised manuscript received 22 April 2009; published 20 July 2009)

Time-resolved x-ray imaging techniques have recently demonstrated the capability to probe the magnetic switching of nanoscale devices. This technique has enabled, for example, the direct observation of the nonuniform intermediate states assumed by the magnetic free layer during reversal by a spin-polarized current. These experiments have shown an interesting size-dependent behavior associated with the motion of vortices to mediate the magnetization reversal which cannot be explained by the macrospin picture of spin-torque switching. In this paper we present both experimental and analytical results which show the origin of the complex switching behavior. We use time-resolved x-ray microscopy to further study the switching behavior of samples with 45° angle between the free and polarizing magnetic layers. A model is developed in terms of a linearized Landau-Lifshitz-Gilbert equation showing that the initial dynamics is dominated by the balance between the Oersted field and thermal fluctuations. The spin torque amplifies this dynamics, leading to a strong sensitivity to sample size, angle, and temperature. The model is in good agreement with current and previous experimental observations.

DOI: 10.1103/PhysRevB.80.024417 PACS number(s): 75.60.Jk, 85.75.−d, 75.75.+a

I. INTRODUCTION

Magnetization reversal in nanomagnetic devices due to the spin-transfer torque (STT) effect[1,2] has been experimentally verified by numerous experiments[3–13] and it holds great promise for technological applications such as memory devices and dc current tuned microwave oscillators. Many experimental results[7,10,13] have been interpreted in terms of a single domain rotation model[14–18] for the moving free layer of the device. Over the years increasing evidence has pointed to the presence of nonuniform intermediate states during magnetization reversal[7,19] which have been shown by time-resolved x-ray imaging experiments.[20,21] While early results showed the formation and motion of vortex cores across the sample during magnetization reversal,[22] later experiments in conjunction with micromagnetic simulations revealed an interesting sample size dependence based on unique or degenerate paths of vortex core motion.[23] For "larger" samples (100×180 nm), a vortex core enters and moves across the sample. In smaller samples (110×150 nm and 85×135 nm), a virtual vortex appears to circumvent the sample without entering it. In both cases the magnetization is switched. On the basis of these results, two different types of processes were proposed: deterministic vortex-driven switching (VDS) and stochastic C-state flip-over (CSF) switching. Figure 1 summarizes the model that emerged from the combined experimental and simulation results. The figure also illustrates how a uniform rotation (UR) model may be linked to the other two cases. Switching in this model may be viewed as a special case of the CSF switching with the vortex core remaining far away from the sample edge. The VDS and UR model are seen to represent limiting cases of a unified vortex core switching model.

All experimental and modeling results mentioned above are for samples with collinear geometry, i.e., with magnetization directions in the free and the fixed layers either completely aligned or antialigned. In Sec. II of this paper, we present experimental results of similar time-resolved x-ray imaging experiments performed on samples with a 45° starting angle between the free and the fixed layers. Previously,

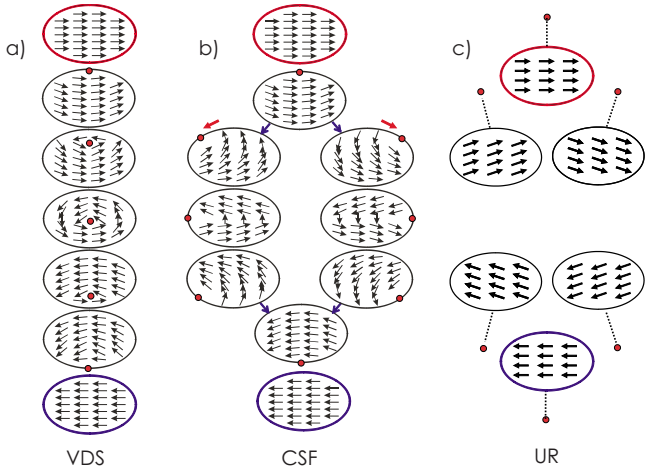

FIG. 1. (Color online) Schematic representation of (a) VDS observed in 100×180 nm samples, (b) CSF mechanism observed for 110×150 nm and 85×135 nm samples, and (c) switching according to the UR model. In all three cases, time proceeds downwards. In (b) two equivalent paths for the motion of the vortex core are possible which makes the switching inherently stochastic, as opposed to the VDS in (a). UR model is shown in (c) for comparing it to CSF in (b).

spin-transfer switching experiments as a function of θ were performed and it was found[24] that the critical current required for switching varied as $1/|\cos\theta|$. The purpose behind performing time-resolved experiments with such sample geometries is to comparatively study the magnetization switching dynamics as a function of θ. In Sec. III, we develop a simple analytical model for explaining the complex magnetization switching behavior observed in experiments. In particular, we derive an expression for the critical sample size, as a function of the angle θ where the switch over between VDS and CSF takes place. In the final Sec. IV, we discuss results of our analytical model in light of all experimental results.

II. EXPERIMENTAL RESULTS

The samples used for this study consist of standard current-perpendicular-to-plane (CPP) spin valve nanopillars. A 2-nm-thick $Co_{0.86}Fe_{0.14}$ film constitutes the free layer. A 3.5 nm Cu film acting as a spacer separates the free layer from the fixed layer which consists of CoFe(1.8)/Ru(0.8)/CoFe(2.0 nm) synthetic antiferromagnet (SAF). The magnetization axis in the SAF is pinned to an underlying IrMn antiferromagnetic (AF) layer. The magnetization axis of the AF is fixed by annealing the deposited magnetic layers in a high external magnetic field. By appropriately choosing the shape of the nanopillar with respect to the pinned AF during the subsequent *e*-beam lithography steps, a suitable angle between the magnetization directions of the free and the fixed layers can be obtained. The details of fabrication process can be found elsewhere.[25] In our case, the designed angle between the free and fixed layers was 45° and we present results on samples with sizes 125×150 nm and 125×200 nm.

The samples were characterized by standard magnetoresistance measurements and hysteric switching between the antiparallel (AP) and parallel (P) states was observed on application of an external magnetic field. The magnetoresistance varies between 25 and 35 $m\Omega$, depending on the exact shape and size of the sample. The samples were also found to switch completely between the AP and P states on application of 4-ns-long current pulses. Typical current densities required for switching are $\approx10^8$ A/cm^2. Such current pulses are used to periodically switch the sample between the AP and P states during our time-resolved x-ray microscopy-based pump-probe experiments. Below we briefly describe our experimental technique. For details, the reader will be referred to our previous publications.

We use time-resolved scanning transmission x-ray microscopy (STXM) technique to study the magnetization dynamics in the free layer of the sample after it is excited by a current pulse. The sample is located on a SiN membrane and is scanned through the 30 nm focus of an x-ray zone plate. The x-rays are produced by a synchrotron source (the Advanced Light Source, in our case) and are incident at an angle of 30° to the sample surface normal. An avalanche photodiode is located behind the sample and it detects the photons transmitted through it. The sample is scanned pixel by pixel through the x-ray focus. For each pixel, the transmitted photons are counted for a fixed integration time to acquire an x-ray absorption image. By taking a difference in the absorption images generated by left and right circularly polarized light, we can extract the magnetic contrast at every pixel in the sample by use of the x-ray magnetic circular dichroism (XMCD) effect. Four ns long alternate positive and negative current pulses are applied to the sample which alternately switch it between two stable states. The current pulses are synchronized to the x-ray photon pulses which appear at a frequency of 500 MHz and whose typical pulse width is 70 ps. The evolution of the magnetization is probed by a series of photon pulses which are counted in different counters. By changing the fine delay between the current pulses and the x-ray pulses, magnetization dynamics in the subnanosecond regime can be probed. The details of the electronics that we built in order to perform these experiments[20,21] and the details of the experimental setup[22] for scanning the sample in a STXM are described in our previous work.

By use of the XMCD effect, one can measure the in-plane magnetization component of the sample that has a nonzero projection along the direction of propagation of the x-ray pulses. We first measure one component (say x) of the magnetization at a specific number of time delays between the current pulses and the x-ray pulses. Then we rotate the sample by 90° in the x-y plane inside STXM to measure the y component of the magnetization at the same time delays. These two set of magnetic contrast images are then combined pixel by pixel to construct a magnetization vector image. The reader is referred to other publications[26,27] for details of the magnetization vector image construction.

The switching dynamics of the free layer in a 125×200 nm sample is shown in Figs. 2 and 3. Magnetization reversal in both directions is found to proceed with the formation and movement of a vortex. Figure 2 shows the snapshots of magnetization reversal during the positive current pulse, which switches it from AP to P state. In this figure and in all which follow, the synchronization between the current pulses and the x-ray pulses is such that the rising edge of the positive pulse corresponds to a time reference of 4 ns and the entire pulse sequence is 16 ns long. After the onset of the current pulse, a vortex core is seen to enter the sample [frame (b)] and the vortex core stays in the sample as long as the current pulse is on. The vortex state is stabilized by the Oersted field from the current and it leaves the sample from the other side after the current is off [frame (h)]. The magnetization in the sample is reversed as a result of the vortex core moving through it. Figure 3 shows the magnetization reversal in the opposite direction (P to AP) during the negative current pulse. Here also we see that the vortex core enters the sample after the current is on [frame (k)] and stays as long as the current is on [frames (k)–(p)] and leaves the sample after the current is off [frame (q)].

Figures 4 and 5 show magnetization switching in a 125×150 nm sample. Switching in this case is quite different than switching in the 125×200 nm sample discussed above. During the negative current pulse (P to AP transition) vortex-driven switching is seen. However, during the AP to P transition, there is no signature of a vortex being present in the free layer at any time. Figure 4 shows the snapshots of mag-

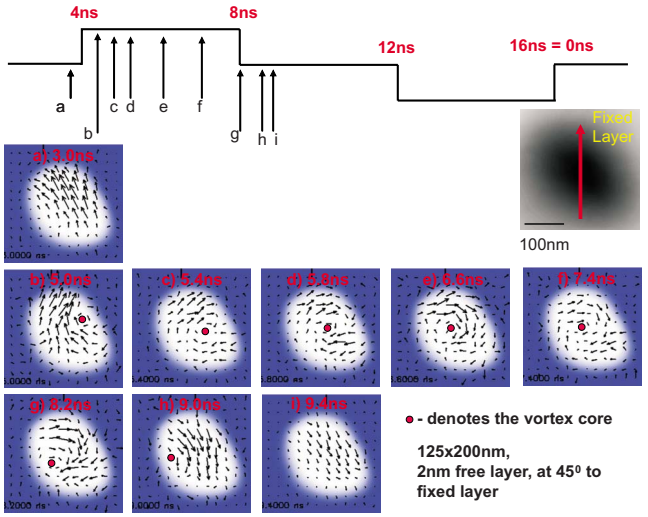

FIG. 2. (Color online) Evolution of the magnetization during the positive pulse in a 125×200 nm sample measured by way of time-resolved scanning transmission x-ray microscopy. The magnetization reversal proceeds via a vortex core moving through the sample. The vortex core stays in the sample as long as the current is on. The figure on the right below the schematic pulse sequence is a STXM image of the sample. The magnetization direction of the fixed layer is shown by the vertical arrow.

netization reversal during the positive current pulse. After the current is turned on, at 5.0 ns [frame (b)], the magnetization appears slightly bent. In the next three frames [(c)–(e)], it is seen that the magnetic contrast almost vanishes. At 5.5 ns [frame (f)], the magnetization in the opposite direction appears and the full magnetization is reached by 6.6 ns [frame (h)]. Figure 5 shows the snapshots of the magnetization reversal in the free layer during the negative current pulse. In this figure we note that the magnetization bends after the onset of the current [frames (i) and (j)] and this leads to the

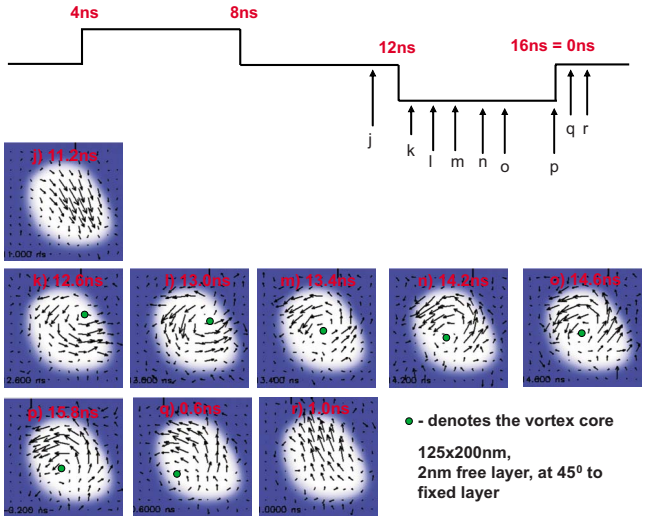

FIG. 3. (Color online) Evolution of the magnetization during the negative pulse in a 125×200 nm sample measured by way of time-resolved scanning transmission x-ray microscopy. The magnetization reversal proceeds via a vortex core moving through the sample. The vortex core stays in the sample as long as the current is on.

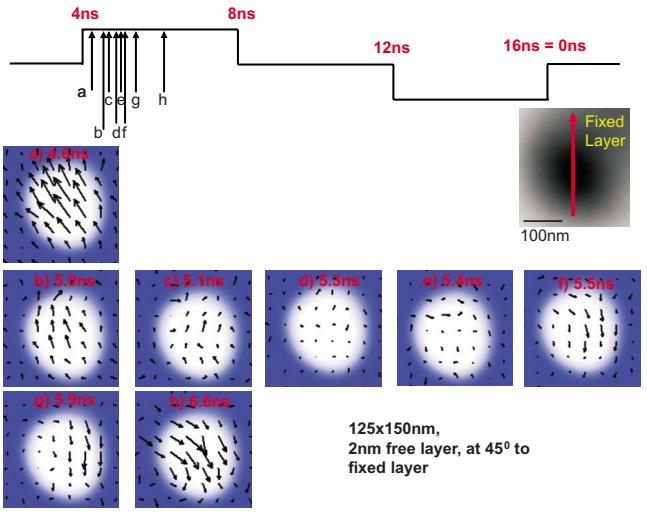

FIG. 4. (Color online) Evolution of the magnetization during the positive pulse in a 125×150 nm sample measured by way of time-resolved scanning transmission x-ray microscopy. The image on the right below the schematic pulse sequence is a STXM image of the sample. The magnetization direction of the fixed layer is shown by the vertical arrow in this image.

formation of the vortex core inside the sample as seen in frames (l)–(n). The vortex core moves out by 13.9 ns [frame (o)], thereby reversing the magnetization. During the negative current pulse, we thus see that the reversal proceeds via a vortex core moving through the sample, unlike during the positive current pulse. The interesting aspect of results on the 125×150 nm sample is that it undergoes a different type of switching for each direction of magnetization reversal. The VDS observed in the 125×200 nm sample and during the negative pulse in the 125×150 nm sample is similar to the reversal process observed in the 110×180 nm samples with no angle between the free and the fixed layers studied

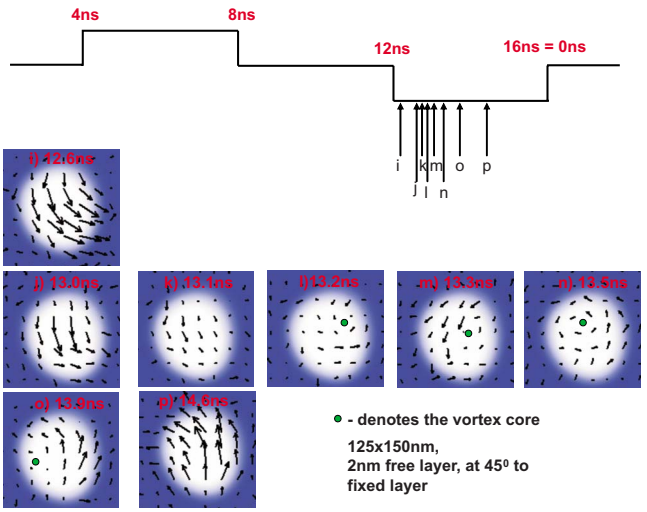

FIG. 5. (Color online) Evolution of the magnetization during the negative pulse in a 125×150 nm sample measured by way of time-resolved scanning transmission x-ray microscopy. The magnetization reversal proceeds via a vortex core moving through the sample, unlike reversal during the positive pulse.

previously.[23] Also, switching during the positive pulse in the 125×150 nm sample is similar to that observed in the 110×150 nm sample studied previously,[23] where the magnetic contrast in the x-ray images was found to reduce in strength. A CSF was proposed to be the switching mechanism in this case. The reduced magnetic contrast is a result of a time averaging effect between two equivalent paths that the magnetization in the free layer can take to reverse its direction.

III. SIMPLE MODEL FOR NONUNIFORM MAGNETIZATION SWITCHING

In our previous work,[23] we performed detailed micromagnetic simulations for understanding the complex magnetization switching mechanisms observed in experiments. In combination with the experimental results presented here, one recognizes a general trend in the switching behavior of samples which depends on its size and the angle between the free and fixed layers. In some cases, the magnetization switches via a vortex and in some without the involvement of a vortex. In this section, we present an analytical approach that aims to obtain an over-arching explanation for the switching behavior observed across a variety of samples. We calculate dynamical eigenmodes excited in the free layer due to the current pulse, which are then amplified due to the STT effect. The nature of eigenmode that dominates at initial times (soon after the rising edge of the current pulse) determines the exact nature of switching that the magnetization undergoes. We find that our analytical model is able to satisfactorily explain, both qualitatively and quantitatively, the different switching mechanisms observed experimentally.

The model treats the magnetization dynamics by a linearized Landau-Lifshitz-Gilbert (LLG) equation to capture the *initial* motion of the magnetization at a given temperature in response to a spin current and the Oersted field of the charge current. The torque induced by the spin-polarized current causes the excitation and amplification of specific magnetic eigenmodes within the free layer of the sample. We assume that the later evolution of the switching process, characterized by large amplitude of the modes and the associated nonlinear behavior, is a consequence of the onset of switching in the linear regime.

We start with the LLG equation to describe the magnetization dynamics. This equation incorporates the influence of STT on the magnetization,

$$\dot{\mathbf{M}} = -\gamma(\mathbf{M} \times \mathbf{H}_{\text{tot}}) + \frac{\alpha}{|M|}(\mathbf{M} \times \dot{\mathbf{M}}) + \frac{\alpha'}{|M|^2}[\mathbf{M} \times (\hat{\mathbf{s}} \times \mathbf{M})], \tag{1}$$

where $\mathbf{H}_{\text{tot}}$ is the total magnetic field acting on the magnetization and has contributions from the internal fields, the Oersted field ($\mathbf{H}_{\text{Oe}}$), and an external applied field ($\mathbf{H}_{\text{ext}}$) which is zero in our case. $\hat{\mathbf{s}}$ is a unit vector pointing along the direction of the spin polarization of the electrons entering the free layer. In the linear regime, the deviation of the magnetization from the easy axis is relatively small and therefore the conditions $M_x \approx M_s$ and $M_y, M_z \ll M_s$ are valid, where M_s is the saturation magnetization. In other words, we consider the situation in the free layer immediately after the rising edge of the current pulse. In the linear regime, the internal fields are also approximated by a linear term

$$\mathbf{H}_{\text{int}}(x,y) = \begin{pmatrix} -D_x M_x \\ -D_y M_y \\ -D_z M_z \end{pmatrix}, \tag{2}$$

where D are linear operators on the local magnetization $M(x,y)$. The internal fields $\vec{H}_{\text{int}}$ depend on the magnetization $\vec{M}$ as $\vec{H}_{\text{int}}(x,y) = \vec{H}_{\text{int}}\{\vec{M}\}$. This relation is very complex as each component of the internal fields depends on the magnetization distribution everywhere. Linearization of $\vec{H}_{\text{int}}$ leads to three linear functionals $H_i = H_i\{\vec{M}\}$, $i = x, y, z$ mapping the magnetization distribution to a field distribution. The internal field acts as a restoring field for the magnetization distribution. We now look at the components of H_{int} individually. The z component restores the magnetization if there is an out-of-plane component of M. In a thin magnetic sample and as long as the length scale of the excitations is longer than the film thickness, H_z can be approximated by $-n_z M_z$, where n_z is a constant.

The initial magnetization distribution M_0 is assumed uniform along the x axis. Small changes in the magnetization in the y,z direction only quadratically influence M_x. Therefore linearization of H_x leads to $-n_x M_s$ which is independent of the magnetization distribution. H_y is the restoring field for magnetization deviations from the uniform state along the y direction. Linear approximation leads to $H_y = -D_y\{M_y\}$, where D_y is a linear functional on the magnetization distribution M_y. Here we neglect contributions of M_z as the shape anisotropy dictates $M_z \ll M_{y,x}$. Notice that, unlike in the case of H_z, the lateral extension of the sample does not allow for approximating D_y by a constant: the length scale of magnetic excitations is smaller than the lateral extent of the sample. D_y is in principle complex and contains integrals over the magnetic charge distribution. We do not specify any particular expression for D_y since we do not attempt to explicitly solve for its eigenmodes. By retaining D_y as a generic operator, one could also add the contribution of the exchange interaction to it. As will be clear from the discussion that follows, we are mainly interested in finding out the equation of motion for M_y in order to understand the magnetization switching dynamics. Instead of finding out the exact spatial eigenmodes of D_y, for our calculations, we consider the simplest approximate modes that are in line with our experimental results. In our model we neglect any contribution from magnetocrystalline anisotropy, as the magnetic thin films in the sample are known to be polycrystalline in nature.[25] The easy axis due to the shape anisotropy is along the x axis.

For each point (x,y) on the sample the LLG equation needs to be solved: α is the conventional Gilbert damping parameter and $\alpha' = \frac{\mu_B J_e g}{et} \approx \frac{\mu_B J_e \eta}{et}$ represents the effect of spin-transfer torque. μ_B is the Bohr magneton, J_e is the current density, e is the electronic charge, and t is the thickness of the free layer. The parameter g depends on the angle between the fixed and free layers and the spin polarization of the current.[1] For small angles between the free and fixed layers

(the simplified case that we will consider), the angular dependence in g is negligible and can therefore be approximated by the spin polarization η. The spin direction of the incoming electrons from the fixed layer is taken to be at an angle θ with respect to the easy axis.

The Oersted field exists only in the plane of the sample,

$$\mathbf{H}_{\mathrm{Oe}} = \begin{pmatrix} H_x \\ H_y \\ 0 \end{pmatrix}. \tag{3}$$

Within the approximations made above, Eq. (1) reduces to

$$\begin{pmatrix} \dot{M}_x \\ \dot{M}_y \\ \dot{M}_z \end{pmatrix} \approx -\gamma \begin{pmatrix} -M_z H_y \\ n_z M_s M_z + M_z(H_x - n_x M_s) \\ M_s H_y - M_y(H_x - n_x M_s) - D_y\{M_y\} M_s \end{pmatrix} + \alpha \begin{pmatrix} 0 \\ -\dot{M}_z \\ \dot{M}_y \end{pmatrix} + \frac{\alpha'}{M_s} \begin{pmatrix} -\sin\theta M_y \\ -\cos\theta M_y - \sin\theta M_s \\ -\cos\theta M_z \end{pmatrix}. \tag{4}$$

Developing the LLG equation by the eigenfunctions M_i of D_y we find that the equations of motion for $M_y = \sum_i m_i(t) M_i(x,y)$ [in Eq. (4)] reduce to that of a simple harmonic oscillator (SHO)

$$\ddot{m}_i + b\dot{m}_i + \omega_{0,i}^2 m_i = F_y, \tag{5}$$

where b is the damping constant, $\omega_{0,i}$ is the natural frequency of the ith eigenmode and F is the driving force acting on the magnetization. We define the scalar product denoted as $\langle a,b\rangle = \frac{1}{\pi r^2}\int_0^r\int_0^{2\pi} a(\rho,\phi) b(\rho,\phi)\rho d\phi d\rho$ in cylindrical coordinates. The parameters of the harmonic oscillators are given by

$$b = \frac{\alpha\gamma[M_s(1-n_x) + 2(H_x - n_x M_s)] + 2\alpha_1}{1+\alpha^2}, \tag{6}$$

$$\omega_{0,i}^2 \approx \frac{\gamma^2 n_i n_z M_s^2 + \alpha_1^2}{1+\alpha^2}, \tag{7}$$

$$F_y = \frac{\gamma^2 n_z M_s^2 \langle H_y, M_i\rangle - \alpha_1\alpha_2}{1+\alpha^2} = F_{y1} + F_{y2}, \tag{8}$$

where $\alpha_1 = \frac{\alpha' \cos\theta}{M_s}$ and $\alpha_2 = \alpha' \sin\theta$ and n_i is the ith eigenvalue of D_y. b is a combination of the intrinsic positive damping and negative damping due to spin current, $\omega_{0,i}$ is given by the in-plane and out-of-plane anisotropy fields, and F is given by a combination of the Oersted field and the spin torque. The contribution of the spin-current-dependent term to the frequency is negligible.

The solution to the SHO equation is

$$M_y(t) = \sum_i \left(a_i e^{-bt/2} \cos(\omega_{1,i} t + \phi) + \frac{F_y}{\omega_0^2} \right) M_i, \tag{9}$$

where $\omega_{1,i} = \sqrt{\omega_{0,i}^2 - (\frac{b}{2})^2}$. When b is less than zero (i.e., when negative damping exceeds the intrinsic damping), the amplitude of the oscillatory motion increases exponentially. This is the regime in which we are interested and it occurs whenever the current going through the sample is more than the critical current required for switching. Therefore, although we treat the problem in the linear regime, we can identify the situation when switching would occur by looking at the net damping constant. The critical condition for switching that can be imposed in this model would then be $b<0$. This implies

$$\alpha_1 < -\frac{1}{2}\alpha\gamma[M_s(1-n_x) + 2(H_x - n_x M_s)]. \tag{10}$$

This condition gives the critical current density required for switching,

$$|J_e| > \frac{\alpha\gamma e t M_s}{\eta\mu_B \cos\theta}\left[\frac{M_s}{2}(1-n_x) + H_x - n_x M_s\right]. \tag{11}$$

The first term in the bracket is the contribution from the easy-plane anisotropy, the second term is due to an external field, which is only the Oersted field in our case, and the last term is due to the uniaxial shape anisotropy. A similar expression for the critical current density was derived by Sun,[14] also in the linear approximation.

The initial conditions at time $t=0$ are given by the thermal fluctuations. Since the out-of-plane anisotropy dominates over the in-plane anisotropy, the z component of the magnetization due to thermal fluctuations is expected to be negligible compared to the y component. Hence we set $M_y(0) \neq 0$ and $M_z(0)=0$. The initial conditions determine the phase ϕ_i and the amplitude a_i of the oscillatory modes. The driving force for M_y, given by Eq. (8) is a combination of terms due to the Oersted field (F_{y1}) and spin current (F_{y2}). In the Appendix, we will show that F_{y2} is negligible in comparison to F_{y1}. This implies that the driving force is mainly given by the Oersted field, proportional to H_y. The zeroth eigenmode M_0 has no node and for symmetry reasons its projection onto the Oersted field H_y is zero. Therefore it is only driven by thermal fluctuations. M_0 is similar to the uniform mode and can easily be thermally excited. The excitation is given by $\frac{1}{2}\mu_0 n_0 a_0^2 V = k_B T$, where μ_0 is the permeability of free space, k_B is the Boltzmann constant, and V is the volume of the free layer.

The first eigenmode M_1 has one node and therefore shows the largest overlap with the Oersted field. Assuming it is only excited by the Oersted field (see the Appendix) we obtain an amplitude of $a_1 \approx \frac{F_{y1}}{\omega_{01}^2}$ and $F_{y1} = \frac{\gamma^2 n_z M_s^2 \langle H_y, M_1\rangle}{1+\alpha^2}$. In order to simplify the calculations we write $H_y(x,y) = H_{\max} h_y(x,y)$ with $H_{\max} = \frac{J_e}{2} r$ being the Oersted field at the edge of the pillar. Thus $a_1 \approx \frac{J_e r}{2n_1}\langle h_y, M_1\rangle$. The overlap integral $\langle h_y, M_i\rangle$ is a dimensionless constant.

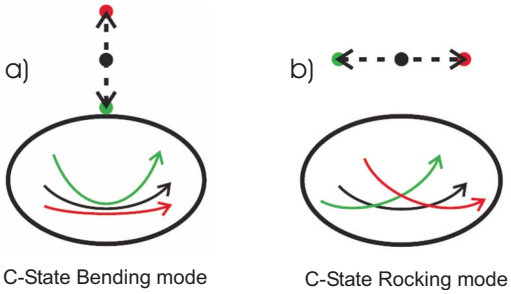

FIG. 6. (Color online) Schematic representation of the (a) C-state bending mode and (b) C-state rocking mode. Also shown are displacements of virtual vortex cores.

Summing up the first two modes, the collective motion of the elements will be like an oscillating C state which is also rocking about the central pivot. We identify the collective motion to be a superposition of this oscillatory C-state type of motion which we call the "C-state bending mode" (corresponding to M_1) and a rocking C-state (corresponding to M_0) type of motion which we call the "C-state rocking mode." The C-state bending and rocking modes are separately shown in Fig. 6. The bending mode can be described by a virtual vortex core moving up and down and the rocking mode can be described by a virtual vortex core moving sideways.[23] Growth of the bending mode will eventually lead to the vortex core entering the sample and thereby cause VDS, whereas the rocking mode will lead to switching by CSF. Since the solution to the LLG equation that we are considering is valid only in the linear regime, i.e., at times close to $t=0$, by using this model, we analyze which of the above-mentioned mode dominates in this regime and predict how the switching would proceed at later times. If the C-state bending mode dominates initially, then the sample would switch by a vortex core moving through it and if the C-state rocking mode dominates, switching would proceed by C-state flip over.

By comparing the rates of growth for the two modes at initial times, we derive an expression for the critical sample size where the switching behavior changes. The rate of growth of a particular mode ($|d(a_i e^{-bt/2})/dt|$) is simply equal to $|a_i(b/2)|$. Thus the comparison between the rates of growth for the two modes reduces to a comparison of their amplitudes of motion at time $t=0$.

A comparison of the amplitudes of the zeroth and the first mode yields the critical condition for reversal by vortex motion. The critical condition is basically a balance condition between the strength of the Oersted field and the strength of thermal fluctuations. The critical condition reduces to the following expression for the critical radius:

$$r_{\text{crit}}^2 \approx \left(\frac{4\cos\theta}{t\langle h_y, M_1\rangle}\right)\left(\frac{\mu_B \eta n_1}{\alpha\gamma M_s^2 e}\right)\sqrt{\frac{2k_B T}{\mu_0 n_0 \pi t}}. \qquad (12)$$

For samples smaller than the critical size, the rocking mode (due to thermal fluctuations) dominates and hence the switching would proceed by CSF, whereas for samples bigger than the critical size, the bending mode (due to Oersted field) dominates and hence would undergo VDS. The change over from one type of switching to another takes place due to the competition between the Oersted field and thermal fluctuations. For example, if only the sample size was to be reduced, everything else remaining unchanged, the influence of thermal fluctuations would increase (due to reduced volume) in comparison to that of the Oersted field (due to reduced radius), and the sample would undergo switching by CSF instead of VDS.

IV. DISCUSSION AND SUMMARY

In order to compare the result of our analytical model with experiments, we choose the following material parameters to get an estimate for the critical size. $M_s=15$ kOe (1.5 T), $\alpha=0.01$, $n_0=0.02$, $\eta=0.3$, $\theta=0$, and $t=2$ nm. The value of n_0 is chosen such that the field required to bring the magnetization along the hard direction is 300 Oe, which is close to the corresponding value measured for our samples. We approximate $n_0 \approx n_1$ as the frequency of backward volume magnetostatic spin waves have a weak dependence on the wave number.[28] The zeroth eigenmode is assumed to be $M_0=1$, representing the uniform mode. The first eigenmode is approximated to be $M_1=\frac{2}{r}x$, which represents the C-state bending observed experimentally. Notice that the prefactors are chosen such that the eigenmodes are normalized. This leads to $\langle h_y, M_1\rangle=\frac{1}{4}$. Together with the standard values for μ_0, μ_B, γ, and e, these parameters yield the critical diameter d_{crit} to be ≈ 155 nm. From our previous work,[23] one can deduce that the experimentally observed value of the critical sample size is close to 150 nm. The numerical estimate of the critical sample size in our model is thus found to be in good agreement with experimental results. We also note that the inverse thickness dependence of the critical size is consistent with experimental observations since 100×150 nm samples with 4-nm-thick free layer switched by motion of vortex cores,[22] whereas the same size samples with 2-nm-thick free layer did not.[23]

The $\cos\theta$ dependence in Eq. (12) originates from the expression for the critical current required for switching. For samples with a nonzero angle between the free and the fixed layers, the critical current for switching the magnetization is higher than that required to switch a similar size sample in the zero degree configuration.[24] Although the torque in the beginning is higher in the former case, it decreases as the angle between the free and the fixed layers reduces with time and therefore the overall efficiency of switching due to spin transfer is lower than in the zero degree configuration. Higher current density for switching implies higher Oersted field which stabilizes a vortex state. This implies that in the noncollinear geometry, VDS should be observable at sample sizes which are smaller than those in the collinear geometry. The experimental results presented here are consistent with this conclusion since VDS is observed in 125×150 nm samples. Higher current density for switching also explains why we observe the vortex state to be present in 125×200 nm sample as long as the current pulse is on.

By analogy to the results obtained previously,[23] it is reasonable to assume that the 125×150 nm sample must be switching by CSF during the positive current pulse. For the

45° case therefore, the critical size for switching seems to be very close to the 125×150 nm samples studied here. We attribute the different switching mechanism observed during positive and negative current pulses to the slight difference in the spin polarization of the current in the two directions. Further experimental studies on similar samples with varying angles between the free and fixed layers and on samples with a wider distribution of sizes would be necessary to conclusively determine the influence of spin polarization on the switching mechanism.

Finally, we also note that the model gives a prediction for the temperature dependence of the critical sample size. Due to the influence of thermal fluctuations, the temperature dependence enters into the expression for the critical radius which implies that with the lowering of temperature, VDS should be observable in smaller samples. This result can be tested by temperature-dependent x-ray imaging experiments in future.

To summarize, we have studied magnetization switching dynamics in spin-transfer torque driven CPP type spin valve nanopillar samples by employing a time-resolved x-ray microscopy technique. Here, we presented results on samples with 45° starting angle between the free and the fixed layers. A 125×200 nm sample is found to switch by VDS whereas the 125×150 nm sample is found to have a combination of VDS and switching due to CSF. The magnetization switching is qualitatively similar to the switching observed in samples with zero degree configuration. We then presented a model based on magnetic eigenmodes to understand the factors affecting the two different types of switching observed in experiments. The central idea in the model is to study the magnetization dynamics in the free layer by treating the LLG equation in the linear regime. Although the linear regime is valid only at initial times (soon after the rising edge of the current pulse) the magnetization dynamics in this short-time period determines which way the switching will proceed at later times. In this model, the balance between the strength of the Oersted field and the thermal fluctuations of the magnetization determine the switching mechanism. The negative damping torque arising from the spin current does not play a role in determining the switching behavior, rather it amplifies the magnetization dynamics initiated by the thermal fluctuations and the Oersted field. The numerical estimate of the critical sample size for change over from VDS type of switching to CSF type for zero degree samples is in good agreement with experimental results. Experimental results in the 45° case are also qualitatively in agreement with the predictions of the model and further experiments would be necessary for a more accurate confirmation.

ACKNOWLEDGMENTS

The Stanford authors would like to acknowledge U.S. Department of Energy, Office of Basic Energy Sciences for funding their research program. All experiments were performed at the Advanced Light Source (ALS) in Berkeley which is also supported by the above-mentioned funding agency. Additional support was received from the Western Institute of Nanoelectronics. J.P.S. and X.W.Y. also acknowledge support from the ALS.

APPENDIX: TERMS IN THE DRIVING FORCE

In this section, we will show that the second term in the expression for the y component of the driving force is negligible compared to the first term. This amounts to saying that the contribution of the spin-torque term to the driving force is negligible compared to the contribution from the Oersted field.

The first and the second terms, F_{y1} and F_{y2}, respectively, are

$$F_{y1}=\frac{\gamma^2 n_z M_s^2\langle H_y,M_i\rangle}{1+\alpha^2}, \tag{A1a}$$

$$F_{y2}=-\frac{\alpha_1\alpha_2}{1+\alpha^2}, \tag{A1b}$$

where $\alpha_1=\frac{\alpha'\cos\theta}{M_s}$, $\alpha_2=\alpha'\sin\theta$, and $\alpha'=\frac{\mu_B J_e\eta}{et}$.

Equation (10) gives the critical condition for switching in the linear approximation. Since we are interested in the regime where switching occurs, the minimum value of α_1 which satisfies this condition is given by

$$|\alpha_1|=\frac{1}{2}\alpha\gamma[M_s(1-n_x)+2H_x-2n_xM_s]. \tag{A2}$$

The first term in the bracket $[M_s(1-n_x)]$ is due to the easy-plane anisotropy and it is much larger than the contributions from Oersted field $(2H_x)$ and the in-plane shape anisotropy $(2n_xM_s)$. Typical value of M_s for CoFe free layer is 15 kOe whereas the maximum contribution from Oersted field and the in-plane switching field for our samples is about 1.6 kOe and 300 Oe, respectively. It is therefore reasonable to neglect the last two terms and use the approximate value of $\alpha\gamma M_s/2$ for α_1. Then the ratio of the two terms can be written as

$$\left|\frac{F_{y2}}{F_{y1}}\right|=\frac{\alpha_1^2 M_s\tan\theta}{\gamma^2 n_z M_s^2\langle H_y,M_i\rangle}=\frac{(\alpha\gamma M_s/2)^2 M_s\tan\theta}{\gamma^2 n_z M_s^2\langle H_y,M_i\rangle}$$
$$\approx\frac{\alpha^2 M_s\tan\theta}{4\langle H_y,M_i\rangle}. \tag{A3}$$

For $\theta=0$, this is zero and the second term does not contribute at all. For other values of $\theta\leq45°$, the ratio can be approximated by

$$\left|\frac{F_{y2}}{F_{y1}}\right|\leq\frac{\alpha^2 M_s}{4H_{\max}\langle h_y,M_i\rangle}. \tag{A4}$$

$H_{\max}$ is simply given by $\frac{J_e r}{2}$. For $\alpha=0.01$ and the current density $J_e=2\times10^8$ A/cm^2 and radius of sample $r=50$ nm

$$\left|\frac{F_{y2}}{F_{y1}}\right|\leq10^{-3} \tag{A5}$$

Hence it is safe to neglect F_{y2} in comparison to F_{y1}.

[1] J. C. Slonczewski, J. Magn. Magn. Mater. **159**, L1 (1996).
[2] L. Berger, Phys. Rev. B **54**, 9353 (1996).
[3] M. Tsoi, A. G. M. Jansen, J. Bass, W. C. Chiang, M. Seck, V. Tsoi, and P. Wyder, Phys. Rev. Lett. **80**, 4281 (1998).
[4] J. Z. Sun, J. Magn. Magn. Mater. **202**, 157 (1999).
[5] E. B. Myers, D. C. Ralph, J. A. Katine, R. N. Louie, and R. A. Buhrman, Science **285**, 867 (1999).
[6] F. J. Albert, J. A. Katine, R. A. Buhrman, and D. C. Ralph, Appl. Phys. Lett. **77**, 3809 (2000).
[7] J. Katine, F. J. Albert, R. A. Buhrman, E. B. Myers, and D. C. Ralph, Phys. Rev. Lett. **84**, 3149 (2000).
[8] J. Grollier, V. Cros, A. Hamzic, J. M. George, H. Jaffres, A. Fert, G. Faini, J. B. Youssef, and H. Legall, Appl. Phys. Lett. **78**, 3663 (2001).
[9] F. J. Albert, N. C. Emley, E. B. Myers, D. C. Ralph, and R. A. Buhrman, Phys. Rev. Lett. **89**, 226802 (2002).
[10] S. I. Kiselev, J. C. Sankey, I. N. Krivorotov, N. C. Emley, R. J. Schoelkopf, R. A. Buhrman, and D. C. Ralph, Nature (London) **425**, 380 (2003).
[11] R. H. Koch, J. A. Katine, and J. Z. Sun, Phys. Rev. Lett. **92**, 088302 (2004).
[12] W. H. Rippard, M. R. Pufall, S. Kaka, S. E. Russek, and T. J. Silva, Phys. Rev. Lett. **92**, 027201 (2004).
[13] I. N. Krivorotov, N. C. Emley, J. C. Sankey, S. I. Kiselev, D. C. Ralph, and R. A. Buhrman, Science **307**, 228 (2005).
[14] J. Z. Sun, Phys. Rev. B **62**, 570 (2000).
[15] Y. B. Bazaliy, B. A. Jones, and S. C. Zhang, Phys. Rev. B **69**, 094421 (2004).
[16] S. E. Russek, S. Kaka, W. H. Rippard, M. R. Pufall, and T. J. Silva, Phys. Rev. B **71**, 104425 (2005).
[17] J. Xiao, A. Zangwill, and M. D. Stiles, Phys. Rev. B **72**, 014446 (2005).
[18] M. Gmitra and J. Barneś, Appl. Phys. Lett. **89**, 223121 (2006).
[19] T. Devolder, A. Tulapurkar, Y. Suzuki, C. Chappert, P. Crozat, and K. Yamagi, J. Appl. Phys. **98**, 053904 (2005).
[20] Y. Acremann, V. Chembrolu, J. P. Strachan, T. Tyliszczak, and J. Stöhr, Rev. Sci. Instrum. **78**, 014702 (2007).
[21] J. P. Strachan, V. Chembrolu, X. W. Yu, T. Tyliszczak, and Y. Acremann, Rev. Sci. Instrum. **78**, 054703 (2007).
[22] Y. Acremann, J. P. Strachan, V. Chembrolu, S. D. Andrews, T. Tyliszczak, J. A. Katine, M. J. Carey, B. M. Clemens, H. C. Siegmann, and J. Stöhr, Phys. Rev. Lett. **96**, 217202 (2006).
[23] J. P. Strachan, V. Chembrolu, Y. Acremann, X. W. Yu, A. A. Tulapurkar, T. Tyliszczak, J. A. Katine, M. J. Carey, M. R. Scheinfein, H. C. Siegmann, and J. Stöhr, Phys. Rev. Lett. **100**, 247201 (2008).
[24] F. B. Mancoff, R. W. Dave, N. D. Rizzo, T. C. Eschrich, B. N. Engel, and S. Tehrani, Appl. Phys. Lett. **83**, 1596 (2003).
[25] D. Lacour, J. A. Katine, N. Smith, M. J. Carey, and J. R. Childress, Appl. Phys. Lett. **85**, 4681 (2004).
[26] J. P. Strachan, Ph.D. thesis, Stanford University, 2007.
[27] V. Chembrolu, Ph.D. thesis, Stanford University, 2008.
[28] K. Y. Guslienko, R. W. Chantrell, and A. N. Slavin, Phys. Rev. B **68**, 024422 (2003).